Tonkie Khimicheskie Tekhnologii = Fine Chemical Technologies.
2025;20(4):344–356 ISSN 2686-7575 (Online)

Chemistry and technology of inorganic materials
Химия и технология неорганических материалов

*UDC 546.03, 54.057*
*https://doi.org/10.32362/2410-6593-2025-20-4-344-356*
*EDN PPMBCK*



RESEARCH ARTICLE

# Cr-substituted M-type hexaferrite solid solutions with high level of substitution

**Alena R. Zykova[1], Andrey I. Kovalev[1,✉], Darya P. Sherstyuk[1], Vladimir E. Zhivulin[1], Sergey V. Taskaev[2], Denis A. Vinnik[1,3,4]**

[1] *Laboratory of Single Crystal Growth, South Ural State University National Research University, Chelyabinsk, 454080 Russia*

[2] *Chelyabinsk State University, Chelyabinsk, 454001 Russia*

[3] *Moscow Institute of Physics and Technology (State University), Dolgoprudny, 141700 Russia*

[4] *St. Petersburg State University, St. Petersburg, Peterhof, 198504 Russia*

✉ *Corresponding author, e-mail: kovalev-andrey-i@mail.ru*

## Abstract

**Objectives.** This study aims to synthesize strontium hexaferrites having a high level of chromium substitution ($SrFe_{12-x}Cr_xO_{19}$, $x = 0–6$) and investigate their structural, morphological, and magnetic properties.

**Methods.** The synthesis was carried out using the solid-phase reaction method at a temperature of 1400°C. The impact of chromium substitution for iron on the phase, structure, morphology, and magnetic characteristics was studied using powder X-ray diffraction (XRD), scanning electron microscopy (SEM), energy-dispersive X-ray spectroscopy, and vibrating-sample magnetometry.

**Results.** XRD analysis confirmed the development of single-phase samples having a hexagonal space group $P6_3/mmc$. An increase in Cr concentration leads to a decrease in unit cell parameters, due to the smaller ionic radius of $Cr^{3+}$. The surface morphology of the samples consists of bulk crystallites a few microns in length. Substitution with Cr results in decreased saturation and remanent magnetization.

**Conclusions.** Pure samples of Cr-substituted strontium hexaferrite were synthesized. The linear dependence of the investigated structural parameters on the Cr concentration confirms the Cr substitution into the hexaferrite solid solution by Vegard's law. In addition to structural parameters, magnetic characteristics were obtained for hexaferrite solid solutions. Saturation and remanent magnetization dependencies were shown to significantly decrease with Cr concentration, while coercive force varies in a complex dependence on Cr concentration. The sample with $x = 1$ has the highest product of coercive force and saturation magnetization, indicating its suitability for permanent magnet application.

**Keywords**

strontium hexaferrites, structure, XRD, SEM, DSC, vibrating-sample magnetometry

**Submitted:** 18.11.2024
**Revised:** 24.01.2025
**Accepted:** 23.05.2025

**For citation**

Zykova A.R., Kovalev A.I., Sherstyuk D.P., Zhivulin V.E., Taskaev S.V., Vinnik D.A. Cr-substituted M-type hexaferrite solid solutions with high level of substitution. *Tonk. Khim. Tekhnol. = Fine Chem. Technol*. 2025;20(4):344–356. https://doi.org/10.32362/2410-6593-2025-20-4-344-356

НАУЧНАЯ СТАТЬЯ

# Твердые растворы гексаферритов M-типа с высокой степенью замещения Cr

**А.Р. Зыкова[1], А.И. Ковалев[1,✉], Д.П. Шерстюк[1], В.Е. Живулин[1], С.В. Таскаев[2], Д.А. Винник[1,3,4]**

[1] *Южно-Уральский государственный университет (национальный исследовательский университет), Челябинск, 454080 Россия*

[2] *Челябинский государственный университет, Челябинск, 454001 Россия*

[3] *Московский физико-технический институт (национальный исследовательский университет), Долгопрудный, 141700 Россия*

[4] *Санкт-Петербургский государственный университет, Санкт-Петербург, Петергоф, 198504 Россия*

✉ *Автор для переписки, e-mail: kovalev-andrey-i@mail.ru*

**Аннотация**

**Цели.** Работа нацелена на синтез стронциевых гексаферритов с высокой степенью замещения железа хромом и исследование их структурных, термических, морфологических и магнитных свойств.

**Методы.** Синтез образцов проводился по твердофазному методу при температуре 1400°C. Влияние замещения железа хромом на фазовый состав, структуру, морфологию и магнитные характеристики синтезированных гексаферритов исследовано методами рентгеновской дифракции, сканирующей электронной микроскопии, энергодисперсионной рентгеновской спектроскопии и вибрационной магнитометрии.

**Результаты.** Анализ методом рентгеновской дифракции показал, что полученные образцы однофазные и соответствуют гексагональной структуре с пространственной группой $P6_3/mmc$. С ростом концентрации хрома размеры элементарной ячейки уменьшаются, что происходит из-за меньшего ионного радиуса иона $Cr^{3+}$. Морфология поверхности образцов показывает присутствие крупных частиц, размером в несколько микрон. Замещение железа хромом приводит к снижению остаточной намагниченности и намагниченности насыщения.

**Выводы.** Однофазные образцы Cr-замещенных стронциевых гексаферритов получены твердофазным методом. Структурные параметры образцов линейно зависят от концентрации Cr, что подтверждает замещение хромом в твердых растворах гексаферритов из-за соблюдения правила Вегарда. В дополнение к структурным параметрам, изучены магнитные характеристики твердых растворов. Для остаточной намагниченности и намагниченности насыщения наблюдается значительное снижение с ростом концентрации Cr. Коэрцитивная сила носит сложный характер зависимости от концентрации Cr. Образец со степенью замещения $x = 1$ обладает наибольшим произведением намагниченности насыщения и коэрцитивной силы, что подчеркивает его применимость в качестве постоянного магнита.

**Ключевые слова**

гексаферриты стронция, структура, рентгеновская дифракция, сканирующая электронная микроскопия, дифференциальная сканирующая калориметрия, вибрационная магнитометрия

**Поступила:** 18.11.2024
**Доработана:** 24.01.2025
**Принята в печать:** 23.05.2025

**Для цитирования**

Zykova A.R., Kovalev A.I., Sherstyuk D.P., Zhivulin V.E., Taskaev S.V., Vinnik D.A. Cr-substituted M-type hexaferrite solid solutions with high level of substitution. *Tonk. Khim. Tekhnol. = Fine Chem. Technol.* 2025;20(4):344–356. https://doi.org/10.32362/2410-6593-2025-20-4-344-356

## INTRODUCTION

Ferrites are an important class of materials, playing a significant role in magnetic applications and high frequency electronics [1–5]. Among them, a subclass of M-type hexagonal ferrites has attracted the research attention due to their unique properties: a Curie temperature of about 450°C, a high corrosion resistance, low production costs, a magnetocrystalline anisotropy of 17.5 kOe, and low dielectric loss [6–9]. Barium hexaferrite ($BaFe_{12}O_{19}$) was the first investigated M-type hexaferrite. This material was used in permanent magnet manufacturing along with strontium hexaferrite ($SrFe_{12}O_{19}$), which is more easily manufacturable, as well as offering higher coercivity ($H_c$) and remanence magnetization ($M_r$), which are important permanent magnet characteristics [10].

Barium and strontium hexaferrites are still used for permanent magnet manufacturing, however,

due to the interest in the M-type hexagonal ferrites structure, proposed hexaferrite applications include photocatalysis [11, 12] and electromagnetic interference shielding [13–15]. Many different hexaferrite solid solutions have been synthesized and investigated using various methods. Mono- or polysubstituted $BaFe_{12}O_{19}$ with Sr [16], Al [17], Ca [18], Ti [19], Mn [20], Ni [21], Gd [22], Cr [23], etc. atoms have been reported, as well as high entropy solid solutions [24–26].

In the scientific literature on hexaferrite, relatively few works have focused on partially $Cr^{3+}$ substituted barium hexaferrite [27–32]. From analyzing these sources, it can be seen that $Cr^{3+}$ substituted barium hexaferrite was earlier synthesized by sol–gel [27–31] and solid-state [32] methods. In the works [27–29], the level of $Cr^{3+}$substitution ($x$) varies from 0.25 to 1, while the synthesis temperature lies in the range from 850 to 1000°C. However, the obtained samples were subject to impurity constraints, consisting not only in the target $BaCr_xFe_{(12-x)}O_{19}$ phase, but also in α-$Fe_2O_3$ [27] and $Cr_2O_3$ [28, 29]. In work [28], the authors were able to obtain single-phase samples of $BaCr_xFe_{(12-x)}O_{19}$ with $x$(Cr) = 0.1–0.8. An increase in Cr concentration was shown to lead to lower saturation magnetization and higher coercive force values. Single-phase samples were also obtained in [31], where $x$(Cr) = 0, 0.5, 1.0, 2.0. The synthesis of pure barium hexaferrite with $x$(Cr) = 2 by the solid-state method was reported in the work [32]; the synthesis process was carried out for 3 h at a temperature of 1300°C.

Concluding the literature review, it becomes clear that the synthesis of single-phase of partially Cr-substituted barium hexaferrite remains problematic. Meanwhile, strontium hexaferrite has not been investigated in terms of Cr substitution. At the same time, an interest in Cr-substituted hexaferrites could be identified in the analyzed publications.

The present study set out to obtain single-phase samples of M-type Sr hexaferrites $SrFe_{(12-x)}Cr_xO_{19}$ with $x$ from 0 to 6 and investigate their magnetic, structural, and morphological properties.

## MATERIALS AND METHODS

### Sample preparation

The samples were prepared using solid-state synthesis. Iron oxide ($Fe_2O_3$), chromium oxide ($Cr_2O_3$), and strontium carbonate ($SrCO_3$) were used as initial components for synthesis. All of the components were reagent-grade (*Reahim*, Russia). They were weighed at a given stoichiometric ratio and ground in an agate mortar (*Rushim*, Russia). Table 1 shows the chemical formula of the samples as well as the mass content of the initial components.

**Table 1.** Compositions of the initial mixture

| No. | Chemical formula | Mass ratio of the initial components, g | | |
|---|---|---|---|---|
| | | $SrCO_3$ | $Fe_2O_3$ | $Cr_2O_3$ |
| 1 | $SrFe_{11.5}Cr_{0.5}O_{19}$ | 1.3374 | 8.3183 | 0.3442 |
| 2 | $SrFe_{11}Cr_1O_{19}$ | 1.3398 | 7.9706 | 0.6897 |
| 3 | $SrFe_{10.5}Cr_{1.5}O_{19}$ | 1.3421 | 7.6216 | 1.0363 |
| 4 | $SrFe_{10}Cr_2O_{19}$ | 1.3445 | 7.2714 | 1.3842 |
| 5 | $SrFe_{9.5}Cr_{2.5}O_{19}$ | 1.3468 | 6.9199 | 1.7332 |
| 6 | $SrFe_9Cr_3O_{19}$ | 1.3492 | 6.5673 | 2.0836 |
| 7 | $SrFe_{8.5}Cr_{3.5}O_{19}$ | 1.3516 | 6.2133 | 2.4351 |
| 8 | $SrFe_8Cr_4O_{19}$ | 1.3539 | 5.8582 | 2.7879 |
| 9 | $SrFe_{7.5}Cr_{4.5}O_{19}$ | 1.3563 | 5.5017 | 3.1419 |
| 10 | $SrFe_7Cr_5O_{19}$ | 1.3587 | 5.1441 | 3.4972 |
| 11 | $SrFe_{6.5}Cr_{5.5}O_{19}$ | 1.3612 | 4.7851 | 3.8537 |
| 12 | $SrFe_6Cr_6O_{19}$ | 1.3636 | 4.4249 | 4.2116 |

After grinding, the mixture was pressed into tablets with a diameter of 8 mm and a height of 5 mm using a hydraulic laboratory press FFMP-15T (*KARALTAY*, Russia) and a metal mold with a force of 5 t/cm$^2$.

The samples were placed on a platinum substrate and sintered in a self-made tube furnace with silicon carbide heaters. Solid-state synthesis lasted for 5 h at 1400°C.

### Phase, structural, microstructural, and elemental analysis

The samples obtained through chemical reaction were studied via powder X-ray diffraction (XRD) analysis (Ultima IV powder diffractometer with CuKα radiation, *Rigaku*, Japan), scanning electron microscopy (SEM), and elemental microanalysis.

The phase content and cell parameters were studied at 25°C. The unit cell parameters were calculated by the Rietveld method using the PDXL software (*Rigaku*, Japan) application. The chemical composition and microstructure images were examined using the scanning electron microscope JEOL JSM-7001F (*JEOL*, Japan) with an energy dispersive X-ray fluorescence spectrometer Oxford INCA X-max 80 (United Kingdom).

Histograms of the distribution of grain sizes were created by using ImageJ (*National Institutes of Health*, USA) and Origin (*OriginLab Corporation*, USA) software.

## Magnetic analysis methods

In order to determine the magnetic parameters, a Quantum Design PPMS® VersaLab vibrating-sample magnetometer (USA) with a magnetic field strength up to 30 kOe at temperatures from 50 to 300 K was used.

## RESULTS AND DISCUSSION

### XRD analysis

The phase composition and unit cell parameters of the samples were determined through powder X-ray diffraction. Figure 1 shows the XRD patterns of single-phase samples. The red strips represent the data for unsubstituted strontium hexaferrite $SrFe_{12}O_{19}$ [33]. Figure 1 shows that the reflections in the XRD patterns of the samples correspond to pure $SrFe_{12}O_{19}$ from the ICDD® database[1] with the hexagonal space group $P6_3/mmc$. On the presented magnified capture of XRD patterns (Fig. 2), it can be clearly observed that the peak positions are shifting to the higher 2θ angle with the introduction of Cr into the hexaferrite.

Unit cell parameters for each obtained solid solution were obtained by indexing the XRD patterns (Table 2).

When Fe in strontium hexaferrite is substituted with Cr, the values of unit cell parameters monotonically decreasing with $x$ (Fig. 3). Since the ionic radius of $Cr^{3+}$ (0.615 Å, CN = 6) is smaller than that of $Fe^{3+}$ (0.645 Å, CN = 6)[2], the unit cell and its parameters decrease with $x$.

**Table 2.** Unit cell parameters of the obtained solid solutions

| Sample composition | Cell sizes | | $c/a$ | Cell volume $V$, Å$^3$ |
|---|---|---|---|---|
| | $a$, Å | $c$, Å | | |
| $SrFe_{12}O_{19}$ [34] | 5.8840 | 23.0500 | 3.9174 | 690.403 |
| $SrFe_{12}O_{19}$ | 5.881(2) | 23.049(9) | 3.9192 | 690.43(5) |
| $SrFe_{11.5}Cr_{0.5}O_{19}$ | 5.875(3) | 23.015(1) | 3.9174 | 687.8867(1) |
| $SrFe_{11}Cr_1O_{19}$ | 5.874(3) | 23.007(1) | 3.9167 | 687.441(6) |
| $SrFe_{10.5}Cr_{1.5}O_{19}$ | 5.870(4) | 22.983(5) | 3.9153 | 685.746(2) |
| $SrFe_{10}Cr_2O_{19}$ | 5.868(1) | 22.968(1) | 3.9141 | 684.897(2) |
| $SrFe_{9.5}Cr_{2.5}O_{19}$ | 5.864(4) | 22.944(2) | 3.9126 | 683.281(1) |
| $SrFe_9Cr_3O_{19}$ | 5.858(2) | 22.930(3) | 3.9143 | 681.519(4) |
| $SrFe_{8.5}Cr_{3.5}O_{19}$ | 5.858(8) | 22.919(6) | 3.9124 | 681.102(2) |
| $SrFe_8Cr_4O_{19}$ | 5.857(6) | 22.875(3) | 3.9055 | 679.748(1) |
| $SrFe_{7.5}Cr_{4.5}O_{19}$ | 5.853(1) | 22.843(6) | 3.9028 | 677.627(1) |
| $SrFe_7Cr_5O_{19}$ | 5.852(2) | 22.828(3) | 3.9009 | 677.075(1) |
| $SrFe_{6.5}Cr_{5.5}O_{19}$ | 5.847(1) | 22.794(2) | 3.8984 | 674.858(2) |
| $SrFe_6Cr_6O_{19}$ | 5.845(8) | 22.776(3) | 3.8966 | 673.849(7) |

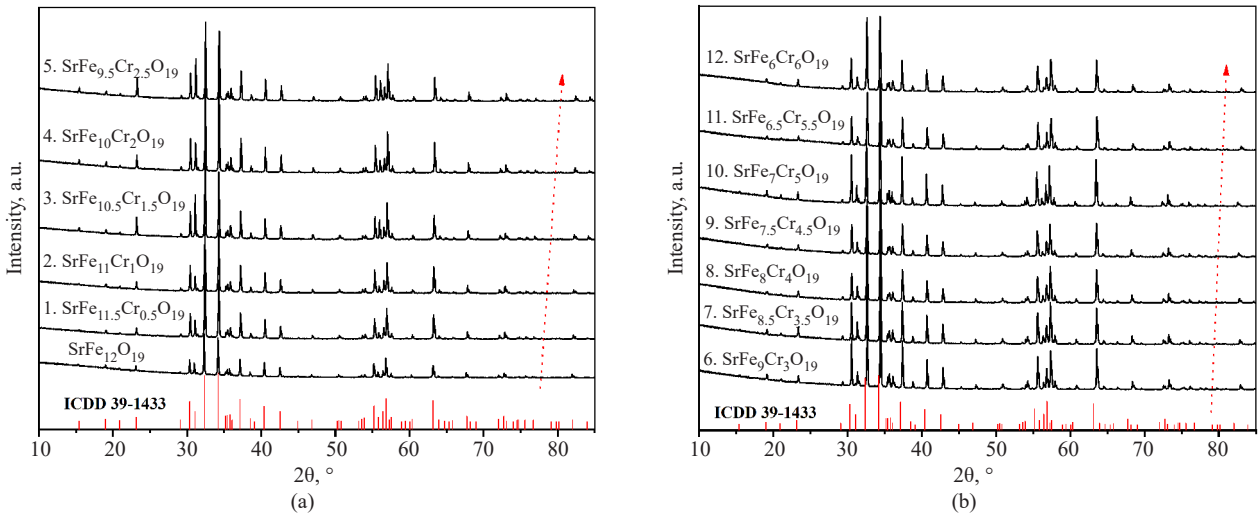


**Fig. 1.** XRD patterns of $SrFe_{12-x}Cr_xO_{19}$ system: (a) $x$ = 0–2.5; (b) $x$ = 3–6

[1] The International Centre for Diffraction Data (ICDD®). https://www.icdd.com/. Accessed July 15, 2024.

[2] Imperial College London, Radii for All Species. http://abulafia.mt.ic.ac.uk/shannon/radius.php. Accessed July 15, 2024.

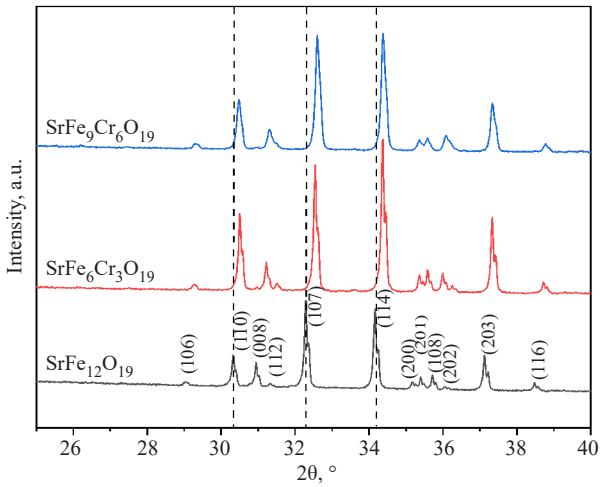


**Fig. 2.** XRD patterns of $SrFe_{12-x}Cr_xO_{19}$ system ($x$ = 0, 3, 6) magnified image

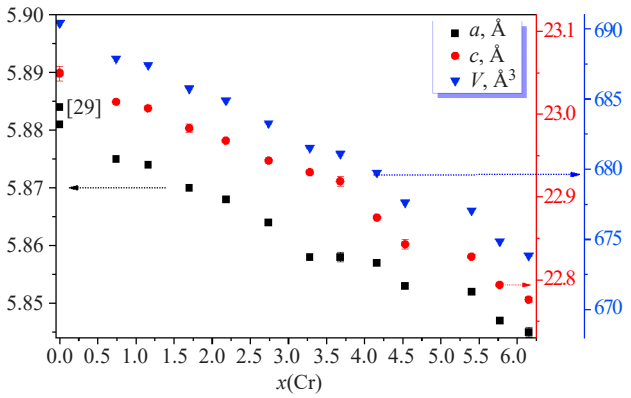


**Fig. 3.** Dependence of the unit cell parameters $a$, $c$, and $V$ on $x$ in $SrFe_{(12-x)}Cr_xO_{19}$

The linear dependence indicates Vegard's law, which confirms the formation of the substitutional solid solutions.

## Surface morphology and elemental composition

The surface morphology of the samples is represented by a multitude of differently oriented crystallites merged together, some of them showing hexagonal morphology. Figures 4a–4l show SEM images of each sample.

From the particle size distribution shown in the histograms, it is evident that particle size is not strongly dependent on the degree of Cr substitution. However, among all the samples, the sample with $x = 6$ stands out; at this rate of substitution, a maximum of 9.4 μm is observed. Results of elemental analysis are presented at Table 3.

## Magnetic properties

Hysteresis loops for $SrFe_{(12-x)}Cr_xO_{19}$ ($x$ = 0–6) solid solutions are shown in Figs. 5 and 6. By visually analyzing the hysteresis loops, we can conclude that Cr concentration ($x$) increases the coercive force ($H_c$), while residual magnetization ($M_r$) and saturation magnetization ($M_s$) both decrease.

**Table 3.** Elemental composition of the samples

| No. | Theoretical chemical formula | Elemental composition of the obtained samples, At. % | | | Resulting chemical formula |
|---|---|---|---|---|---|
| | | Sr | Fe | Cr | |
| 1 | $SrFe_{11.5}Cr_{0.5}O_{19}$ | 1.00 | 11.26 | 0.74 | $SrFe_{11.26}Cr_{0.74}O_{19}$ |
| 2 | $SrFe_{11}Cr_1O_{19}$ | 1.00 | 10.84 | 1.16 | $SrFe_{10.84}Cr_{1.16}O_{19}$ |
| 3 | $SrFe_{10.5}Cr_{1.5}O_{19}$ | 1.00 | 10.30 | 1.70 | $SrFe_{10.30}Cr_{1.70}O_{19}$ |
| 4 | $SrFe_{10}Cr_2O_{19}$ | 1.00 | 9.82 | 2.18 | $SrFe_{9.82}Cr_{2.18}O_{19}$ |
| 5 | $SrFe_{9.5}Cr_{2.5}O_{19}$ | 1.00 | 9.26 | 2.74 | $SrFe_{9.26}Cr_{2.74}O_{19}$ |
| 6 | $SrFe_9Cr_3O_{19}$ | 1.00 | 8.72 | 3.28 | $SrFe_{8.72}Cr_{3.28}O_{19}$ |
| 7 | $SrFe_{8.5}Cr_{3.5}O_{19}$ | 1.00 | 8.32 | 3.68 | $SrFe_{8.32}Cr_{3.68}O_{19}$ |
| 8 | $SrFe_8Cr_4O_{19}$ | 1.00 | 7.84 | 4.16 | $SrFe_{7.84}Cr_{4.16}O_{19}$ |
| 9 | $SrFe_{7.5}Cr_{4.5}O_{19}$ | 1.00 | 7.47 | 4.53 | $SrFe_{7.47}Cr_{4.53}O_{19}$ |
| 10 | $SrFe_7Cr_5O_{19}$ | 1.00 | 6.60 | 5.40 | $SrFe_{6.60}Cr_{5.40}O_{19}$ |
| 11 | $SrFe_{6.5}Cr_{5.5}O_{19}$ | 1.00 | 6.23 | 5.77 | $SrFe_{6.23}Cr_{5.77}O_{19}$ |
| 12 | $SrFe_6Cr_6O_{19}$ | 1.00 | 5.85 | 6.15 | $SrFe_{5.85}Cr_{6.15}O_{19}$ |

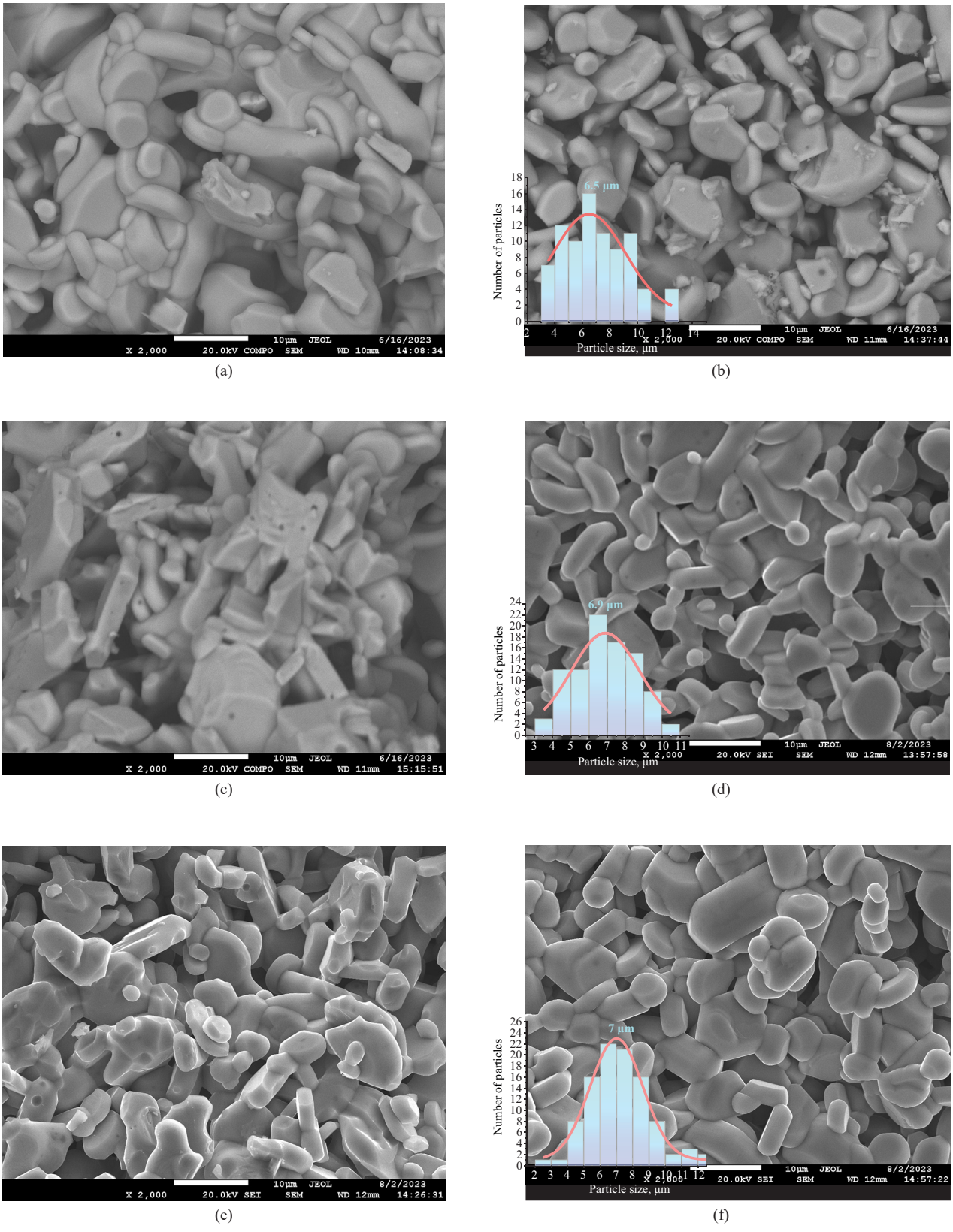


**Fig. 4.** SEM images of $SrFe_{(12-x)}O_{19}$ ceramic samples. $x$ = (a) 0.5; (b) 1.0; (c) 1.5; (d) 2.0; (e) 2.5; (f) 3.0

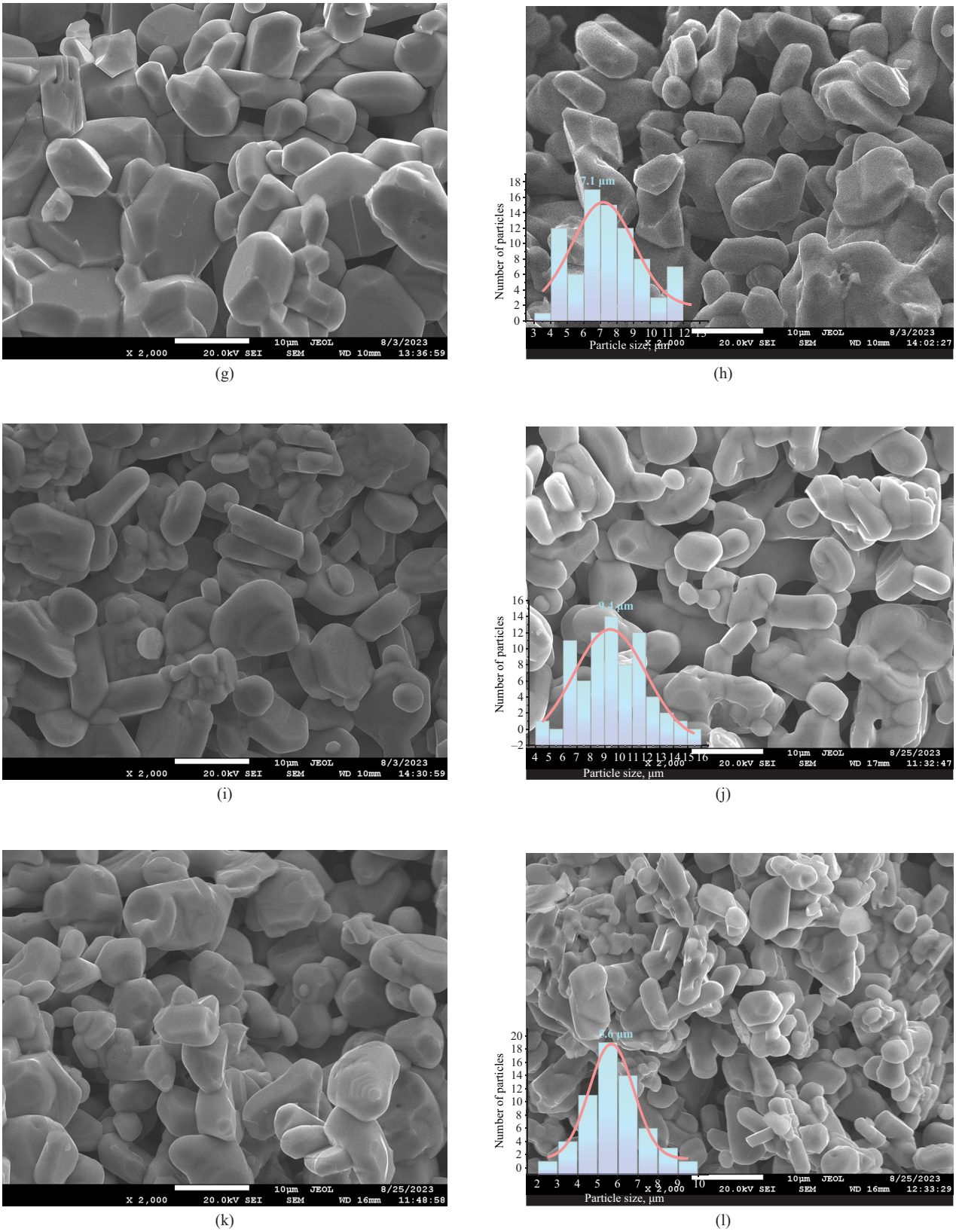


**Fig. 4.** SEM images of $SrFe_{(12-x)}O_{19}$ ceramic samples. $x$ = (g) 3.5; (h) 4.0; (i) 4.5; (j) 5.0; (k) 5.5; (l) 6.0

While this correlates with the data given in [28], the coercive force values for $BaFe_{11.5}Cr_{0.5}O_{19}$ and $SrFe_{11.5}Cr_{0.5}O_{19}$ are not similar at the same level of substitution; this dissimilarity may be attributed to the coercive force being influenced by the nature of the bivalent ion. Since applying 30 kOe to the samples did not cause saturation or the magnetization value to keep increasing, the law to approach saturation was applied. According to the Stoner–Wohlfarth model, $M_s$ can be determined by plotting magnetization ($M$) against $1/H^2$ (Eq. 1) and then extrapolating the linear plot to a zero value of $1/H^2$ (Fig. 7).

The effective magnetic anisotropy constant ($K_{eff}$) can also be determined from this graph by calculating the slope value to determine parameter $B$ (Eq. 2). From this parameter, the value of the magnetic anisotropy field ($H_a$) can be derived (Eq. 3).

$$M = M_s \cdot \left(1 - \frac{B}{H^2}\right), \quad (1)$$

$$K_{eff} = M_s \cdot \sqrt{\frac{15B}{4}}, \quad (2)$$

$$H_a = 2 \cdot \frac{K_{eff}}{M_s}. \quad (3)$$

The values of $M_r$ and $H_c$ are determined from hysteresis loops (Figs. 5 and 6). The values of $M_s$ are presented in Table 4; $K_{eff}$ and $H_a$ values are presented in Table 5. With a temperature decrease, $H_c$ decreases but $M_s$ and $M_r$ increase. $M_s$ and $M_r$ linearly depend on the Cr concentration (Figs. 9 and 10). $H_c$ does not fit perfectly to the linear dependence, but demonstrates a more complicated fit. This could be caused by the complex $Cr^{3+}$ ion substitution for $Fe^{3+}$ ions in different Wyckoff positions.

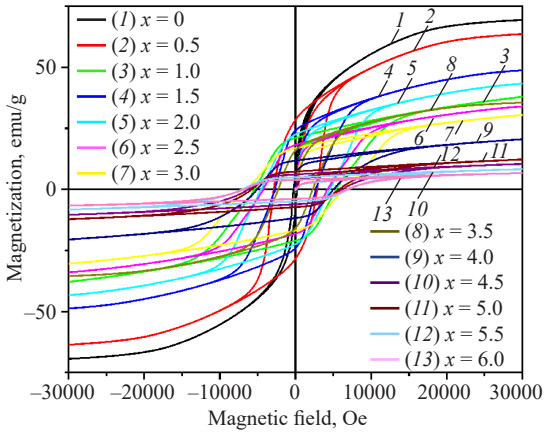


**Fig. 5.** Hysteresis loops of $SrFe_{(12-x)}Cr_xO_{19}$ ($x$ = 0.5–6.0) for solid solutions at 300 K

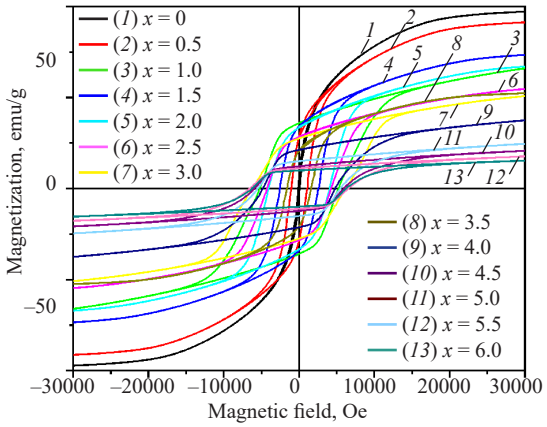


**Fig. 6.** Hysteresis loops of $SrFe_{(12-x)}Cr_xO_{19}$ ($x$ = 0.5–6.0) solid solutions at 50 K

**Table 4.** Magnetic parameters of $SrFe_{(12-x)}Cr_xO_{19}$ ($x$ = 0–6) solid solutions

| $x$ (Cr) | 300 K | | | 50 K | | |
|---|---|---|---|---|---|---|
| | $M_s$, emu/g | $M_r$, emu/g | $H_c$, Oe | $M_s$, emu/g | $M_r$, emu/g | $H_c$, Oe |
| 0 | 67.90 | 21.03 | 610 | 99.76 | 5.95 | 95 |
| 0.5 | 66.14 | 28.49 | 2868 | 94.19 | 28.69 | 1105 |
| 1.0 | 41.04 | 21.02 | 5414 | 71.25 | 35.90 | 5245 |
| 1.5 | 51.93 | 24.09 | 2683 | 77.30 | 34.00 | 2553 |
| 2.0 | 46.48 | 22.44 | 4514 | 71.41 | 33.36 | 4050 |
| 2.5 | 36.58 | 18.19 | 4204 | 58.61 | 28.33 | 4247 |
| 3.0 | 32.79 | 16.85 | 6491 | 54.68 | 27.47 | 6216 |
| 3.5 | 37.27 | 15.97 | 2282 | 54.32 | 20.66 | 1596 |
| 4.0 | 22.18 | 11.74 | 5061 | 40.46 | 21.22 | 4804 |
| 4.5 | 11.33 | 6.09 | 6201 | 22.44 | 12.23 | 5935 |
| 5.0 | 13.34 | 7.26 | 5771 | 26.59 | 15.05 | 5537 |
| 5.5 | 9.12 | 4.91 | 7037 | 19.20 | 11.12 | 6575 |
| 6.0 | 7.37 | 3.89 | 6800 | 16.73 | 9.93 | 6278 |

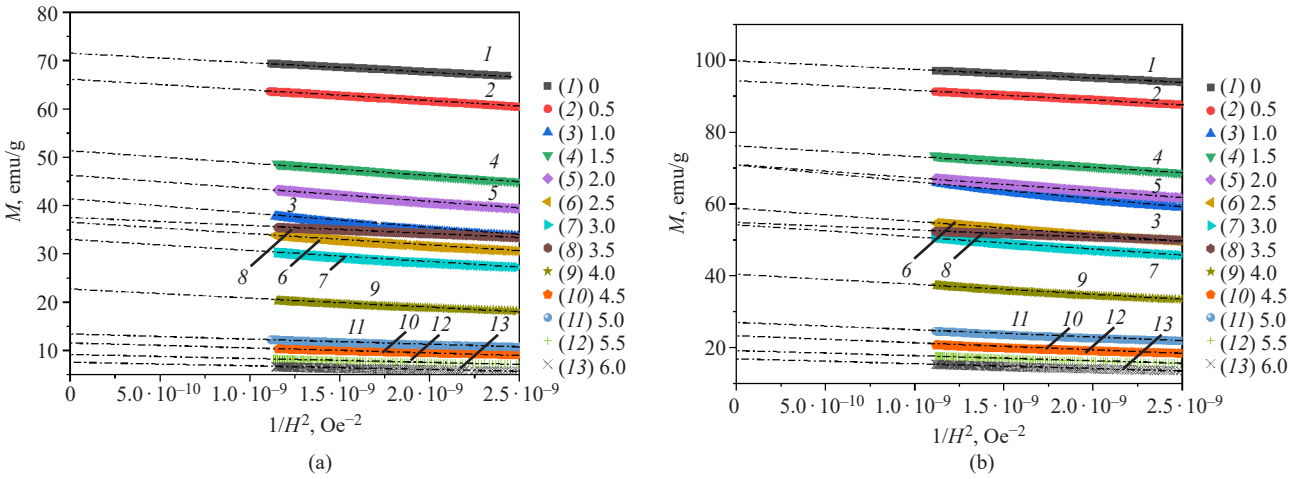


**Fig. 7.** Dependencies of magnetization on the magnetic field for (a) 300 K; (b) 50 K

An analysis of field cooling (FC) magnetization curves (Fig. 8) reveals a mostly linear growth of magnetization with cooling. However, the sample with $x = 0.5$ shows a nonlinear dependence with a peak. This could be related to the redistribution of the resulting magnetic moment due to complex $Cr^{3+}$ ion substitution.

**Table 5.** Parameters of magnetic anisotropy $SrFe_{(12-x)}Cr_xO_{19}$ ($x$ = 0–6), solid solutions

| $x$ (Cr) | 300 K | | 50 K | |
|---|---|---|---|---|
| | $K_{eff} \cdot 10^{-6}$ emu/g·Oe | $H_a$, Oe | $K_{eff} \cdot 10^{-6}$ emu/g·Oe | $H_a$, Oe |
| 0 | 0.70 | 20756 | 0.94 | 18773 |
| 0.5 | 0.75 | 22742 | 0.96 | 20465 |
| 1.0 | 0.69 | 33399 | 1.17 | 32900 |
| 1.5 | 0.74 | 28618 | 1.00 | 25908 |
| 2.0 | 0.71 | 30736 | 1.03 | 28783 |
| 2.5 | 0.59 | 31991 | 0.90 | 30756 |
| 3.0 | 0.53 | 32504 | 0.88 | 32028 |
| 3.5 | 0.47 | 25024 | 0.60 | 22055 |
| 4.0 | 0.37 | 33543 | 0.67 | 33051 |
| 4.5 | 0.20 | 34696 | 0.38 | 33550 |
| 5.0 | 0.23 | 34999 | 0.44 | 33395 |
| 5.5 | 0.17 | 36561 | 0.33 | 33964 |
| 6.0 | 0.14 | 37108 | 0.29 | 34377 |

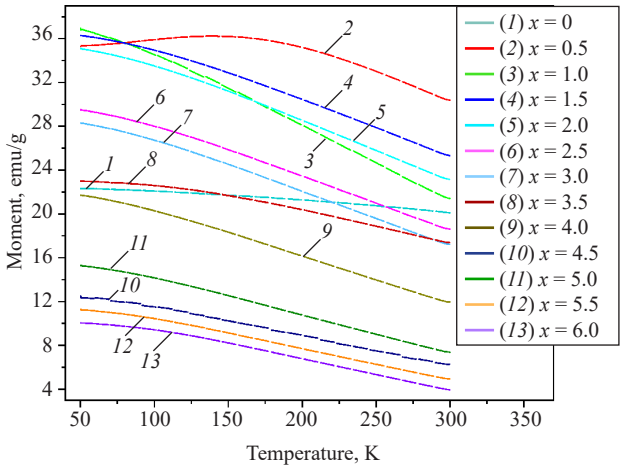


**Fig. 8.** Field cooling at 500 Oe magnetization curves of $SrFe_{(12-x)}Cr_xO_{19}$ ($x$ = 0–6), solid solutions

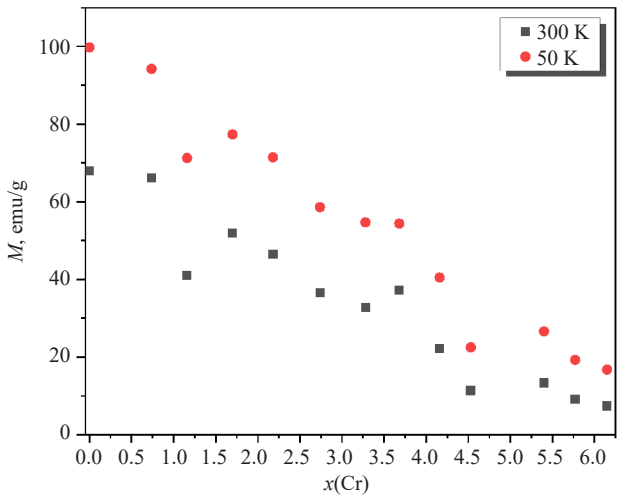


**Fig. 9.** Dependence of saturation magnetization ($M_s$) on Cr content at 50 and 300 K

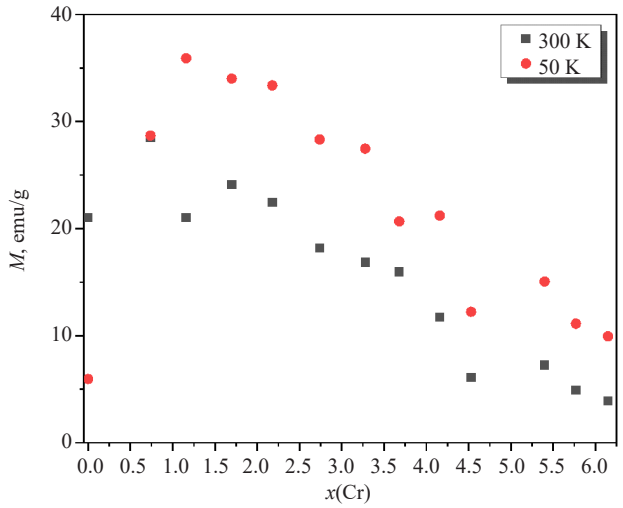


**Fig. 10.** Dependence of remanent magnetization ($M_r$) on Cr content at 50 and 300 K

The replacement of Fe by Cr in hexaferrite strontium leads to complex changes in the magnetic structure, which ultimately reduces the saturation magnetization of the material. This change can be explained in terms of the replacement of $Fe^{3+}$ (5 μB) ions by less magnetic $Cr^{3+}$ (3 μB) ions in octahedral and tetrahedral positions, which results in a decrease in the total magnetic moment per unit volume of material to weaken exchange interactions.

## CONCLUSIONS

$SrFe_{(12-x)}Cr_xO_{19}$ solid solutions with $x$ up to 6 were synthesized using the ceramic method. Average crystallite sizes varied from 5.6 to 9.4 μm. The purity of the samples was verified using XRD analysis: all obtained samples consists only of crystal structure, which is isomorphic to magnetoplumbite. The linear dependence of the investigated structural parameters $a$, $c$, and $V$ on the Cr concentration confirms the incorporation of Cr into the hexaferrite solid solution according to Vegard's law. In addition to structural parameters, magnetic characteristics were obtained for hexaferrite solid solutions. A trend for $M_s$ and $M_s$ dependencies to significantly decrease with Cr concentration is observed. Coercive force shows a complex dependence on Cr concentration. The sample with $x$ = 1 has the highest product of $M_s$ and $H_c$, indicating its high magnetic potential and suitability for use in the manufacture of permanent magnets. Samples with high Cr substitution ($x$ = 5.5, 6.0) possess the highest $H_c$ values, which is a favorable parameter for high-frequency applications; however, additional investigation on other parameters is needed. Cr substituted ferrites can be utilized at high-frequency electronic or sensor production.

## Acknowledgments

The study was supported by the Russian Science Foundation (project No. 24-29-20187, http://rscf.ru/project/24-29-20187).

## Authors' contributions

**A.R. Zykova**—conceptualization, formal analysis, funding acquisition, investigation, methodology, supervision.

**A.I. Kovalev**—formal analysis, investigation.

**D.P. Sherstyuk**—formal analysis, investigation.

**V.E. Zhivulin**—methodology, resources.

**S.V. Taskaev**—formal analysis, investigation.

**D.A. Vinnik**—conceptualization, methodology, project administration, resources, supervision.

*The authors declare no conflict of interest.*

## REFERENCES

1. Khudaysh L., Ahmed I.A., Ejaz S.R., Khan S.A., Haleem Y.A., Ibrahim M.M., Ali M., Farid H.M.T, El-Bahy Z.M. Analysis of cerium substitution in Co–Sr based spinel ferrites for high frequency application. *J. Rare Earths*. 2023;42(9):1755–1763. https://doi.org/10.1016/j.jre.2023.10.013
2. He D., Xu Z., Wang K., Wu P., Cui J., Qiao L., Wang T. The regulation of high-frequency magnetic properties of NiZnCo ferrite for miniaturized antenna application. *J. Magn. Magn. Mater.* 2023;588(15):171449. https://doi.org/10.1016/j.jmmm.2023.171449
3. El Yaagoubi M., Schrödl M., Schwegler D., Münster B. Development of hard ferrite filled thermoplastic elastomers for the production of permanent magnets. *Sensors Actuators A Phys.* 2022;333(1):113224. https://doi.org/10.1016/j.sna.2021.113224
4. Waki T., Nakai S., Tabata Y., Nakamura H. Role of oxygen potential in dopant solubility in ferrite magnets: Enhanced Zn solubility and magnetization in La–Zn co-substituted magnetoplumbite-type strontium ferrite. *Mater. Res. Bull.* 2023;168:112470. https://doi.org/10.1016/j.materresbull.2023.112470
5. Icin K., Akyol S., Alptekin F., Yıldız A., Sünbül S.E., Ergin İ., Öztürk S. A comparative study of the correlation among the phase formation, crystal stability and magnetic properties of $SrFe_{12-x}M_xO_{19}$ (M=$Al^{3+}$, $Cr^{3+}$ and $Mn^{3+}$, $x$ = 0–0.5) ferrite permanent magnets. *J. Solid State Chem.* 2023;324:124126. https://doi.org/10.1016/j.jssc.2023.124126

6. Hashim M., Salih S.J., Ismail M.M., Ahmed A., Meena S.S., Gaikwad A.A., Jotania R.B., Kumar S., Ravinder D., Kumar R., Imran A., Batoo K.M., Shirsath S.E. Effect of lightly substituted samarium ions on the structural, optical, magnetic and dielectric properties of the sonochemically synthesized M-type Sr-hexaferrite nanoparticles. *Phys. B: Condens. Matter*. 2024;681:415840. https://doi.org/10.1016/j.physb.2024.415840
7. Rambabu C., Aruna B., Shanmukhi P.S.V., Gnana Kiran M., Murali N., Mammo T. Wegayehu, Parajuli D., Choppara P., Himakar P., Lakshmi Narayana P.V. Effect of $La^{3+}/Cu^{2+}$ and $La^{3}/Ni^{2+}$ substitution on the synthesis, magnetic and dielectric properties of M−type $Sr_{1-x}La_xFe_{12-x}M_xO_{19}$ (M = Cu and Ni) hexaferrite. *Inorg. Chem. Commun.* 2024;159:111753.
8. Gorbachev E.A., Lebedev V.A., Kozlyakova E.S., Alyabyeva L.N., Ahmed A., Cervellino A., Trusov L.A. Tuning the microstructure, magnetostatic and magnetodynamic properties of highly Al-substituted M-type Sr/Ca hexaferrites prepared by citrate-nitrate auto-combustion method. *Ceram. Int.* 2023;49(16):26411–26419. https://doi.org/10.1016/j.ceramint.2023.05.177
9. Yao Y., Hrekau I.A., Tishkevich D.I., Zubar T.I., Turchenko V.A., Lu S., Silibin M.V., Migas D.B., Sayyed M.I., Trukhanov S.V., Trukhanov A.V. Correlation of the chemical composition, phase content, structural characteristics and magnetic properties of the Bi-substituted M-type hexaferrites. *Ceram. Int.* 2023;49(22):37009–37016. https://doi.org/10.1016/j.ceramint.2023.09.033
10. Pullar R.C. Hexagonal ferrites: A review of the synthesis, properties and applications of hexaferrite ceramics. *Prog. Mater. Sci.* 2012;57(7):1191–1334. https://doi.org/10.1016/j.pmatsci.2012.04.001
11. Chandel M., Ghosh B.K., Moitra D., Ghosh N.N. Barium Hexaferrite ($BaFe_{12}O_{19}$) Nanoparticles as Highly Active and Magnetically Recoverable Catalyst for Selective Epoxidation of Styrene to Styrene Oxide. *J. Nanosci. Nanotechnol.* 2018;18(5):3478–3483. https://doi.org/10.1166/jnn.2018.14625
12. Khaliq N., Bibi I., Majid F., Sultan M., Amami M., Iqbal M. Zn and Mn doped $Ba_{1-x}Zn_xFe_{12-y}Mn_yO_{19}$ as highly photoactive under visible light with enhanced electrochemical and dielectric properties. *Mater. Sci. Semicond. Process.* 2022;139:106324. https://doi.org/10.1016/j.mssp.2021.106324
13. Danish M., ul Islam M., Ahmad F., Madni M.N., Jahangeer M. Synthesis of M-type hexaferrite reinforced graphene oxide composites for electromagnetic interference shielding. *J. Phys. Chem. Solids*. 2024;185:111783. https://doi.org/10.1016/j.jpcs.2023.111783
14. Gunanto Y.E., Izaak M.P., Sitompul H., Adi W.A. Composite Paint based on Barium-Strontium-Hexaferrite as an Absorber of Microwaves at X-band Frequency. *Mater. Today Proc.* 2019;13(1):1–4. https://doi.org/10.1016/j.matpr.2019.03.177
15. Chakradhary V.K., Akhtar M.J. Highly coercive strontium hexaferrite nanodisks for microwave absorption and other industrial applications. *Compos. Part B: Eng.* 2020;183:107667. https://doi.org/10.1016/j.compositesb.2019.107667
16. Trukhanov A.V., Turchenko V.A., Kostishin V.G., Damay F., Porcher F., Lupu N., Bozzo B., Fina I., Polosan S., Silibin M.V., Salem M.M., Tishkevich D.I., Trukhanov S.V. The origin of the dual ferroic properties in quasi-centrosymmetrical $SrFe_{12-x}In_xO_{19}$ hexaferrites. *J. Alloys Compd.* 2021;886:161249. https://doi.org/10.1016/j.jallcom.2021.161249
17. Wang X., Yan H., Zhao S., Liu S., Chang H. Modifiable natural ferromagnetic resonance frequency and strong microwave absorption in $BaFe_{12-y-2x}Al_ySn_xMn_xO_{19}$ M-type hexaferrite. *J. Magn. Magn. Mater.* 2023;586:171159. https://doi.org/10.1016/j.jmmm.2023.171159
18. Yousaf M., Nazir S., Hayat Q., Akhtar M.N., Akbar M., Lu Y., Noor A., Zhang J.-M., Shah M.A.K.Y., Wang B. Magneto-optical properties and physical characteristics of M-type hexagonal ferrite ($Ba_{1-x}Ca_xFe_{11.4}Al_{0.6}O_{19}$) nanoparticles (NPs). *Ceram. Int.* 2021;47(8):11668–11676. https://doi.org/10.1016/j.ceramint.2021.01.006
19. Jyotsna K., Phanjoubam S. Improved magnetoelectric coupling of Co–Ti substituted barium hexaferrite at room temperature and related electrical investigations. *Mater. Chem. Phys.* 2024;317:129186. https://doi.org/10.1016/j.matchemphys.2024.129186
20. Dongquoc V., Park S.-Y., Jeong J.-R., Tu B.D., Huong Giang D.T., Dang N.T., Phan T.L. Electronic structure, and dielectric, magnetic and reflection-loss behaviors of $BaFe_{12-x}Mn_xO_{19}$ ($0<x\leq2$) hexaferrites. *J. Magn. Magn. Mater.* 2023;588(8):171486.
21. Cheon S.J., Choi J.R., Lee S., Lee J.I., Lee H. Frequency tunable Ni–Ti-substituted Ba–M hexaferrite for efficient electromagnetic wave absorption in 8.2–75 GHz range. *J. Alloys Compd.* 2024;976:173019. https://doi.org/10.1016/j.jallcom.2023.173019
22. Hashhash A., Hassen A., Baleidy W.S., Refai H.S. Impact of rare-earth ions on the physical properties of hexaferrites $Ba_{0.5}Sr_{0.5}RE_{0.6}Fe_{11.4}O_{19}$, (RE = La, Yb, Sm, Gd, Er, Eu, and Dy). *J. Alloys Compd.* 2021;873:159812. https://doi.org/10.1016/j.jallcom.2021.159812
23. Atif M., Hanif Alvi M., Ullah S., Ur Rehman A., Nadeem M., Khalid W., Ali Z., Guo H. Impact of strontium substitution on the structural, magnetic, dielectric and ferroelectric properties of $Ba_{1-x}Sr_xFe_{11}Cr_1O_{19}$ ($x$ = 0.0–0.8) hexaferrites. *J. Magn. Magn. Mater.* 2020;500:166414. https://doi.org/10.1016/j.jmmm.2020.166414
24. Zhivulin V.E., Trofimov E.A., Zaitseva O. V., Sherstyuk D.P., Cherkasova N.A., Taskaev S.V., Vinnik D.A., Alekhina Y.A., Perov N.S, Naidu K.C.B., Elsaeedy H.I., Khandaker M.U., Tishkevich D.I., Zubar T.I., Trukhanov A.V., Trukhanov S.V. Preparation, phase stability, and magnetization behavior of high entropy hexaferrites. *IScience*. 2023;26(7):107077. https://doi.org/10.1016/j.isci.2023.107077
25. Yao Y., Zhivulin V.E., Zykova A.R., Cherkasova N.A., Vinnik D.A., Trofimov E.A., Gudkova S.A., Zaitseva O.V., Taskaev S.V., Alyabyeva L.N., Gorshunov B.P., Gurchenko A.A., Lu S., Trukhanov S.V., Trukhanov A.V. High entropy $BaFe_{12-x}(Ti/Mn/Ga/In)_xO_{19}$ ($x$ = 1–7) oxides: Correlation of the composition, entropy state, magnetic characteristics, and terahertz properties. *Ceram. Int.* 2023;49(19):31549–31558. https://doi.org/10.1016/j.ceramint.2023.07.106
26. Luo X., Huang S., Huang R., Hong J., Yuan S., Shu Z., Zhao L., Lu C., Jin H. Rare-earth high-entropy magnetoplumbite structure hexaluminates $(La_{1/5}Nd_{1/5}Sm_{1/5}Eu_{1/5}Gd_{1/5})MAl_{11}O_{19}$ (M = Mg, Zn) for thermal barrier coating applications with enhanced mechanical and thermal properties. *Ceram. Int.* 2024;50(12):21281–21288. https://doi.org/10.1016/j.ceramint.2024.03.237
27. Qiu J., Wang Y., Gu M. Effect of Cr substitution on microwave absorption of $BaFe_{12}O_{19}$. *Mater. Lett.* 2006;60(21–22):2728–2732. https://doi.org/10.1016/j.matlet.2006.01.079
28. Ounnunkad S., Winotai P. Properties of Cr-substituted M-type barium ferrites prepared by nitrate–citrate gel-autocombustion process. *J. Magn. Magn. Mater.* 2006;301(2):292–300. https://doi.org/10.1016/j.jmmm.2005.07.003
29. Dhage Vinod N., Mane M.L., Babrekar M.K., Kale C.M., Jadhav K.M. Influence of chromium substitution on structural and magnetic properties of $BaFe_{12}O_{19}$ powder prepared by sol–gel auto combustion method. *J. Alloys Compd.* 2011;509(12):4394–4398. https://doi.org/10.1016/j.jallcom.2011.01.040

30. Qiu J., Gu M., Shen H. Microwave absorption properties of Al- and Cr-substituted M-type barium hexaferrite. *J. Magn. Magn. Mater.* 2005;295(3):263–268. https://doi.org/10.1016/j.jmmm.2005.01.018
31. Kumar S., Supriya S., Kar M. Correlation between temperature dependent dielectric and DC resistivity of Cr substituted barium hexaferrite. *Mater. Res. Express.* 2017;4:126302. https://doi.org/10.1088/2053-1591/aa9a51
32. Bashkirov L.A., Kostyushko Yu.L. Formation of Ferrite-Cromites $BaFe_{10}Cr_2O_{19}$ and $BaFe_{10}Cr_2O_{19}$ in the Solid-Phase reaction of $Fe_2O_3$ and $Cr_2O_3$ with barium or strontium carbonate. *Russ. J. Appl. Chem*. 2005;78:351–355. http://doi.org/10.1007/s11167-005-0294-z [Original Russian Text: Bashkirov L.A., Kostyushko Yu.L. Formation of Ferrite-Cromites $BaFe_{10}Cr_2O_{19}$ and $BaFe_{10}Cr_2O_{19}$ in the Solid-Phase reaction of $Fe_2O_3$ and $Cr_2O_3$ with barium or strontium carbonate. *Zhurnal Prikladnoi Khimii.* 2005;78(3):357–361 (in Russ.).]
33. Wong-Ng W., McMurdie H.F., Paretzkin B., Kuchinski M.A., Dragoo A.L. Standard X-Ray Diffraction Powder Patterns of Fourteen Ceramic Phases. *Powder Diffr.* 1988;3(4):246–254. https://doi.org/10.1017/S0885715600013579
34. Obradors X., Solans X., Collomb A., Samaras D., Rodriguez J., Pernet M., Font-Altaba M. Crystal structure of strontium hexaferrite $SrFe_{12}O_{19}$. *J. Solid State Chem.* 1988;72(2):218–224. https://doi.org/10.1016/0022-4596(88)90025-4

## About the Authors

**Alena R. Zykova,** Cand. Sci. (Chem.), Researcher, Crystal Growth Laboratory, South Ural State University (National Research University) (76, Lenina pr., Chelyabinsk, 454080, Russia). E-mail: zykovaar@susu.ru. Scopus Author ID 57203743055, RSCI SPIN-code 4777-5816, https://orcid.org/0000-0001-6333-5551

**Andrey I. Kovalev,** Postgraduate Student, Department of Materials Science, Physical and Chemical Properties of Materials, South Ural State University (National Research University) (76, Lenina pr., Chelyabinsk, 454080, Russia). E-mail: kovalev-andrey-i@mail.ru. Scopus Author ID 59364557200, RSCI SPIN-code 4221-8845, https://orcid.org/0009-0003-4773-1687

**Darya P. Sherstyuk,** Postgraduate Student, Department of Materials Science, Physical and Chemical Properties of Materials, South Ural State University (National Research University) (76, Lenina pr., Chelyabinsk, 454080, Russia). E-mail: sherstiukd@susu.ru. Scopus Author ID 57208630693, RSCI SPIN-code 1013-4917, https://orcid.org/0000-0002-8461-9761

**Vladimir E. Zhivulin,** Cand. Sci. (Phys.-Math.), Head of the Crystal Growth Laboratory, South Ural State University (National Research University) (76, Lenina pr., Chelyabinsk, 454080, Russia). E-mail: zhivulinve@mail.ru. Scopus Author ID 57044766800, ResearcherID U-50003-2019, RSCI SPIN-code 6282-2773, https://orcid.org/0000-0002-4389-8936

**Sergey V. Taskaev,** Dr. Sci. (Phys.-Math.), Rector, Chelyabinsk State University (129, Brat'ev Kashirinykh ul., Chelyabinsk, 454001, Russia). E-mail: tsv@csu.ru. Scopus Author ID 55886287900, ResearcherID AAU-9890-2021, RSCI SPIN-code 4131-9937, https://orcid.org/0000-0001-6352-2816

**Denis A. Vinnik,** Dr. Sci. (Chem.), Professor, Department of Materials Science, Physical and Chemical Properties of Materials, South Ural State University (National Research University) (76, Lenina pr., Chelyabinsk, 454080, Russia); Leading Researcher-Head of the Laboratory of Semiconductor Oxide Materials, Institute of Quantum Technologies, Moscow Institute of Physics and Technology (9, Institutskii per., Dolgoprudnyi, Moscow oblast, 141700, Russia); Professor, Institute of Chemistry, St. Petersburg University (7–9, Universitetskaya nab., St. Petersburg, 199034, Russia). E-mail: vinnikda@susu.ru. Scopus Author ID 24451310100, ResearcherID K-1594-2013, RSCI SPIN-code 5971-1044, https://orcid.org/0000-0002-5190-9834

## Об авторах

**Зыкова Алена Романовна,** к.х.н., научный сотрудник, лаборатория роста кристаллов, ФГАОУ ВО «Южно-Уральский государственный университет (национальный исследовательский университет) (454080, Россия, Челябинск, пр-т Ленина, д. 76). E-mail: zykovaar@susu.ru. Scopus Author ID 57203743055, SPIN-код РИНЦ 4777-5816, https://orcid.org/0000-0001-6333-5551

**Ковалев Андрей Игоревич,** аспирант, кафедра «Материаловедение и физико-химия материалов», ФГАОУ ВО «Южно-Уральский государственный университет (национальный исследовательский университет) (454080, Россия, Челябинск, пр-т Ленина, д. 76). E-mail: kovalev-andrey-i@mail.ru. Scopus Author ID 59364557200, SPIN-код РИНЦ 4221-8845, https://orcid.org/0009-0003-4773-1687

**Шерстюк Дарья Петровна,** аспирант, кафедра «Материаловедение и физико-химия материалов», ФГАОУ ВО «Южно-Уральский государственный университет (национальный исследовательский университет) (454080, Россия, Челябинск, пр-т Ленина, д. 76). E-mail: sherstiukd@susu.ru. Scopus Author ID 57208630693, SPIN-код РИНЦ 1013-4917, https://orcid.org/0000-0002-8461-9761

**Живулин Владимир Евгеньевич,** к.ф.-м.н., заведующий лабораторией роста кристаллов, ФГАОУ ВО «Южно-Уральский государственный университет (национальный исследовательский университет) (454080, Россия, Челябинск, пр-т Ленина, д. 76). E-mail: zhivulinve@mail.ru. Scopus Author ID 57044766800, ResearcherID U-50003-2019, SPIN-код РИНЦ 6282-2773, https://orcid.org/0000-0002-4389-8936

**Таскаев Сергей Валерьевич,** д.ф.-м.н., ректор, ФГБОУ ВО «Челябинский государственный университет» (454001, Челябинск, ул. Братьев Кашириных, д. 129). E-mail: tsv@csu.ru. Scopus Author ID 55886287900, ResearcherID AAU-9890-2021, SPIN-код РИНЦ 4131-9937, https://orcid.org/0000-0001-6352-2816

**Винник Денис Александрович,** д.х.н., профессор РАН, профессор кафедры «Материаловедение и физико-химия материалов», ФГАОУ ВО «Южно-Уральский государственный университет (национальный исследовательский университет) (454080, Россия, Челябинск, пр-т Ленина, д. 76); ведущий научный сотрудник, заведующий лабораторией полупроводниковых оксидных материалов, Институт квантовых технологий, ФГАОУ ВО «Московский физико-технический университет (национальный исследовательский университет)» (141701, Россия, Московская обл., г. Долгопрудный, Институтский пер., д. 9); профессор, Институт химии, ФГБОУ ВО «Санкт-Петербургский государственный университет» (199034, Россия, Санкт-Петербург, Университетская наб., д. 7-9). E-mail: vinnikda@susu.ru. Scopus Author ID 24451310100, ResearcherID K-1594-2013, SPIN-код РИНЦ 5971-1044, https://orcid.org/0000-0002-5190-9834

*The text was submitted by the authors in English and*
*edited for English language and spelling by Thomas A. Beavitt*